nature neuroscience

Amyloid-β as a positive endogenous regulator of release probability at hippocampal synapses

Efrat Abramov[1,3], Iftach Dolev[1,3], Hilla Fogel[1], Giuseppe D Ciccotosto[2], Eyal Ruff[1] & Inna Slutsky[1]

Accumulation of cerebral amyloid-β peptide (Aβ) is essential for developing synaptic and cognitive deficits in Alzheimer's disease. However, the physiological functions of Aβ, as well as the primary mechanisms that initiate early Aβ-mediated synaptic dysfunctions, remain largely unknown. Here we examine the acute effects of endogenously released Aβ peptides on synaptic transfer at single presynaptic terminals and synaptic connections in rodent hippocampal cultures and slices. Increasing extracellular Aβ by inhibiting its degradation enhanced release probability, boosting ongoing activity in the hippocampal network. Presynaptic enhancement mediated by Aβ was found to depend on the history of synaptic activation, with lower impact at higher firing rates. Notably, both elevation and reduction in Aβ levels attenuated short-term synaptic facilitation during bursts in excitatory synaptic connections. These observations suggest that endogenous Aβ peptides have a crucial role in activity-dependent regulation of synaptic vesicle release and might point to the primary pathological events that lead to compensatory synapse loss in Alzheimer's disease.

© 2009 Nature America, Inc. All rights reserved.

npg

It is now more than a decade since Aβ was first shown to be a normal, soluble product of neuronal metabolism[1–3]. However, its physiological role in neuronal function remains elusive. Aβ is produced by sequential limited proteolysis of the amyloid precursor protein (APP) conducted by two aspartyl proteases, β- and γ-secretase[4,5]. The production and subsequent release of Aβ positively correlate with the level of neuronal and synaptic activity[6,7]. It has been suggested that synaptic vesicle recycling through coupled endo-exocytosis is the primary mechanism that mediates activity-dependent Aβ production and release[7,8]. The concentration of Aβ in the synaptic cleft varies, and at any given time is determined by the balance of Aβ production, release and degradation. Several members of the M13 zinc-dependent metallopeptidase family, such as neprilysin, insulin-degrading enzyme and endothelin-converting enzymes 1 and 2, have been implicated in the degradation of endogenous Aβ in the rodent brain[9,10]. Of these enzymes, neprilysin might be the best candidate for regulating Aβ in the synaptic cleft because of its presynaptic localization[11] and the extracellular position of its catalytic site[12].

Synapse loss is the strongest structural correlate of cognitive decline in patients with Alzheimer's disease[13,14]. Studies on mouse models of Alzheimer's disease provide evidence that soluble Aβ oligomers contribute to the downregulation of synapse density[15–18]. Although these data support a homeostatic role of Aβ in the control of synapse strength and number on a long timescale[6,15], early modifications mediated by Aβ that initiate synaptic dysfunctions remain controversial. Much effort has been directed toward elucidating synaptotoxic Aβ species[18,19]. The ectopic application of specific Aβ peptides has generated highly heterogeneous data, ranging from an increase in spontaneous synaptic activity and intrinsic excitability of neurons[20,21] to a lack of effect on synaptic transmission[18] or even its depression[6,22]. Such inconsistencies suggest that the concentration, molecular composition and oligomeric states of Aβ peptides differentially affect synaptic function. However, it is still not understood how endogenously released Aβ, comprising peptides of different lengths and molecular conformations, regulates synaptic transfer in normal, non-transgenic hippocampal circuits on a fast timescale.

In an attempt to answer this question, we used optical and electrophysiological tools to assess the acute effects of changes in endogenous extracellular Aβ concentration ($[A\beta]_o$) on synaptic transmission during different patterns of neuronal activity in rat hippocampal cultures and in acute hippocampal slices. Our results show that endogenously released Aβ peptides positively regulate the release probability of synapses, but do not alter postsynaptic function or intrinsic neuronal excitability. The relationships between endogenous $[A\beta]_o$, short-term synaptic plasticity, the excitation-inhibition (E/I) balance, and ongoing neuronal activity are examined here.

RESULTS

Inhibition of neprilysin increases release probability

As synaptic vesicle recycling positively regulates $[A\beta]_o$ on a rapid timescale[7,8], we investigated whether endogenously released Aβ would in turn modulate vesicle recycling through a feedback mechanism. To achieve an acute increase in endogenous Aβ in the synaptic cleft we used thiorphan, a competitive inhibitor of the presynaptic rate-limiting peptidase neprilysin[11,23,24] and neprilysin-like metalloendopeptidases[25]. Thiorphan (500 nM, 1 h) significantly increased

[1]Department of Physiology and Pharmacology, Sackler Faculty of Medicine, Tel Aviv University, Tel Aviv, Israel. [2]Department of Pathology, Bio21 Molecular Science and Biotechnology Institute and Mental Health Research Institute, The University of Melbourne, Parkville, Victoria, Australia. [3]These authors contributed equally to this work. Correspondence should be addressed to I.S. (islutsky@post.tau.ac.il).

Received 19 May; accepted 25 September; published online 22 November 2009; doi:10.1038/nn.2433

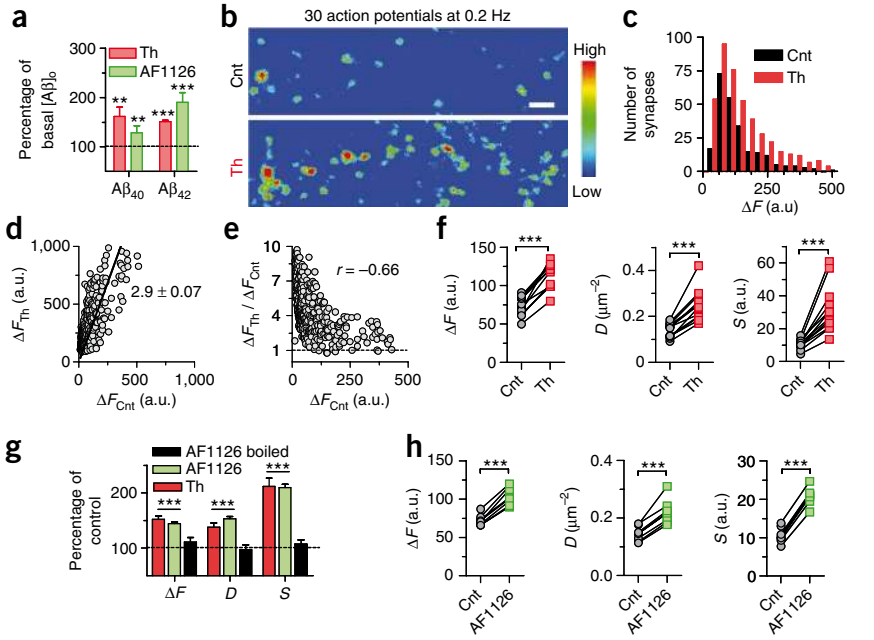

Figure 1 Acute inhibition of neprilysin increases basal synaptic vesicle recycling. (**a**) $[A\beta_{x-40}]_o$ and $[A\beta_{x-42}]_o$ were elevated by application of thiorphan (500 nM, 1 h; $n = 4$, $P < 0.001$ for $A\beta_{42}$ and $P < 0.01$ for $A\beta_{40}$) and AF1126 (5 μg ml^{-1}, 1 h; $n = 4$, $P < 0.001$ for $A\beta_{42}$ and $P < 0.01$ for $A\beta_{40}$). (**b**) Representative high-magnification ΔF images before and 10 min after application of 500 nM thiorphan. Stimulation during FM1-43 staining: 30 action potentials at 0.2 Hz. Scale bar: 2 μm. Fluorescence intensities (arbitrary units, a.u.) are coded using a pseudocolor transformation. (**c**) ΔF histograms before (black bars, Cnt) and after (red bars, Th) thiorphan application in a single experiment. The median ΔF increased from 86 to 142 a.u. and D increased from 254 to 433. (**d**) Thiorphan effect at the single-synapse level. Slope of linear fit is 2.9 ± 0.07. (**e**) Thiorphan-induced augmentation is inversely proportional to the initial presynaptic strength (Spearman $r = -0.66$, $P < 0.0001$, the same data as in **d**). (**f**) Effects of thiorphan on ΔF, D and S across synaptic populations in 12 experiments. (**g**) Average magnitude of the effects produced by a 1-h application of thiorphan ($n = 43$, $P < 0.001$), anti-neprilysin AF1126 antibody ($n = 10$, $P < 0.001$), and heat-denatured AF1126 antibody ($n = 4$, $P > 0.2$) on presynaptic strength. (**h**) Effect of AF1126 antibody on ΔF, D and S ($n = 10$, $P < 0.0001$). Error bars represent ± s.e.m. * $P < 0.05$, ** $P < 0.01$, *** $P < 0.001$.

the concentrations of $A\beta_{x-40}$ and $A\beta_{x-42}$ in the extracellular culture medium ($[A\beta_{40}]_o$ and $[A\beta_{42}]_o$, measured by sandwich ELISA, $n = 4$, $P < 0.01$; **Fig. 1a**). We investigated whether thiorphan acutely affects synaptic vesicle recycling at individual hippocampal synapses using the activity-dependent dye FM1-43 as a marker of synaptic vesicle turnover[26]. We evaluated the functional properties of synapses by estimating the release probability (*Pr*) and spatial distribution of active presynaptic terminals[27,28]. To this end, we quantified the total amount of releasable fluorescence at each bouton (ΔF) and the density of FM^+ puncta per image (D) following stimulation by 30 action potentials at a rate of 0.2 Hz in the presence of 10 μM FM1-43 (**Supplementary Fig. 1**). **Figure 1b** illustrates a typical high-magnification ΔF image (a sub-region of the total imaged area, see **Supplementary Fig. 2**) before and after thiorphan application. The total presynaptic strength within a given region of the hippocampal network (S) can be estimated as the product of ΔF and D ($S = \Delta F \times D$). Single vesicle resolution (**Supplementary Fig. 3** and **Supplementary Discussion**) enables us to convert ΔF to *Pr* and ensures that we detect active terminals that release at least one vesicle per applied 30 action potentials in our experimental system (corresponding to the detection limit of *Pr* ~0.04). Acute application of thiorphan (500 nM, 10 min) induced a substantial increase in both ΔF and D across synaptic populations, resulting in 2.8-fold increase in the total presynaptic strength S (**Fig. 1c**). Analysis of the effect of thiorphan at the single synapse level in the same experiment revealed considerable variability across synapses (**Fig. 1d**,**e**). The degree of thiorphan-induced presynaptic facilitation was inversely correlated to initial ΔF (**Fig. 1e**, Spearman $r = -0.66$, $P < 0.0001$). No correlation was found between presynaptic changes and initial ΔF in a control experiment with two identical successive staining-destaining runs (Spearman $r = -0.02$, $P > 0.5$, **Supplementary Fig. 1**), indicating that the inverse correlation detected for the thiorphan effect was not a statistical artifact. The collective results of these experiments show a profound increase in ΔF, D and, subsequently, S ($n = 12$, $P < 0.0001$, **Fig. 1f**). The EC_{50} of thiorphan for presynaptic enhancement was 47 ± 7 nM (**Supplementary Fig. 2**), of the same order of magnitude as the EC_{50} to increase $[A\beta_{42}]_o$ in our experimental system (28 ± 2 nM; **Supplementary Fig. 2**). The presynaptic effect of thiorphan was reversible and long-lasting (**Supplementary Fig. 2**).

Given that fluorescence quantification based on FM staining depends on exocytosis-endocytosis coupling, we determined the effect of thiorphan on vesicle exocytosis *per se* by measuring the rate of FM destaining during low-frequency stimulation[29]. The experimental protocol described above was modified for staining of the total pool of recycling vesicles by 600 action potentials at 10 Hz and destaining by 1-Hz stimulation (**Supplementary Fig. 4**). Thiorphan increased the destaining rate constant ($k = 1/\tau_{decay}$, where τ_{decay} is an exponential time course) by ~180% ($n = 4$, $P < 0.001$, **Supplementary Fig. 4**), suggesting acceleration of the exocytosis rate. Furthermore, thiorphan was ineffective in increasing presynaptic strength during low-frequency stimulation at a high $[Ca^{2+}]_o$ (four-fold higher than physiological), which caused saturation of synaptic vesicle release in our preparation (**Supplementary Fig. 4**). Together, these results suggest that the acute effect of thiorphan is attributable to an increase in release probability.

To examine whether a selective blockage of neprilysin activity affects synaptic vesicle release, we used the polyclonal AF1126 antibody, which was raised against rodent neprilysin and neutralizes the enzyme's activity. Application of AF1126 (5 μg ml^{-1}, 1 h) triggered an increase in $[A\beta]_o$ (128 ± 14% and 190 ± 20% for $[A\beta_{40}]_o$ and $[A\beta_{42}]_o$, respectively, $n = 4$, $P < 0.001$; **Fig. 1a**) and an increase in presynaptic strength by 209 ± 6% due to an increase in both ΔF and D ($n = 8$, $P < 0.0001$; **Fig. 1h**). The magnitude of the effect of AF1126 was similar to that of thiorphan for an identical application time (1 h, $P > 0.3$, **Fig. 1g**). Heat-denaturated AF1126 had no significant influence on presynaptic activity ($n = 4$, $P > 0.2$; **Fig. 1g**), confirming the molecular specificity of AF1126 in increasing release probability. These results indicate that neprilysin activity negatively regulates basal synaptic vesicle recycling in hippocampal synapses.

© 2009 Nature America, Inc. All rights reserved.

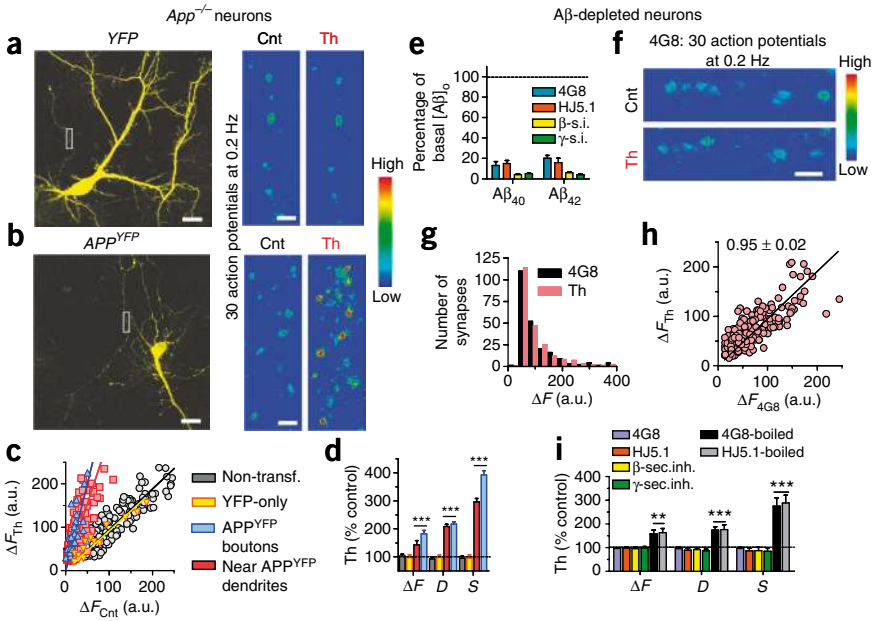

Figure 2 Aβ mediates thiorphan-induced presynaptic enhancement. (**a**) Left: representative images of a YFP-expressing neuron in $App^{-/-}$ culture. Scale bar: 20 μm. Right: high-magnification ΔF images (FM4-64, 15 μM) from axon of the same neuron (white rectangle) before and after thiorphan application. Scale bar: 2 μm. (**b**) As **a**, but for neurons expressing APP^{YFP} in $App^{-/-}$ cultures. (**c**) Single synapse analysis of thiorphan effect in non-transfected $App^{-/-}$ boutons (gray symbols), APP^{YFP}-expressing boutons (blue symbols), non-transfected boutons in the proximity (50 μm) of the APP^{YFP}-expressing dendrites (red symbols) and YFP-only expressing boutons (yellow symbols). (**d**) Average effect of thiorphan ($n = 5$) on presynaptic strength in $App^{-/-}$ cultures for the groups shown in **c**. (**e**) Effects of 4G8 antibody (5 μg ml^{-1}, 1 h), HJ5.1 antibody (5 μg ml^{-1}, 1 h), β-secretase inhibitor (BACE1 inhibitor IV, 0.5 μM, 8 h) and γ-secretase inhibitor (L-685,458, 0.2 μM, 8 h) on $[A\beta_{x-40}]_o$ and $[A\beta_{x-42}]_o$ ($n = 4$, $P < 0.0001$). (**f**) Representative ΔF images (FM1-43, 10 μM) before and after thiorphan application, following pretreatment with 4G8 (5 μg ml^{-1}, 2 h). Scale bar: 2 μm. (**g**) ΔF histograms before and after thiorphan application. (**h**) Single synapse analysis. Slope of linear fit is 0.95 ± 0.02. (**i**) Average effects of thiorphan on ΔF, D and S in Aβ-depleted cultures following pretreatment with 4G8 (5 μg ml^{-1}, $n = 11$, $P > 0.3$) and HJ5.1 (5 μg ml^{-1}, $n = 6$, $P > 0.2$) antibodies, β-secretase inhibitor (0.5 μM, $n = 16$, $P > 0.2$) or γ-secretase inhibitor (0.2 μM, $n = 13$, $P > 0.2$). Heat-denatured 4G8 and HJ5.1 antibodies did not block the thiorphan effect (5 μg ml^{-1}, $n = 4$, $P < 0.001$). Error bars represent ± s.e.m. $^*P < 0.05$, $^{**}P < 0.01$, $^{***}P < 0.001$.

© 2009 Nature America, Inc. All rights reserved.

Aβ mediates thiorphan-induced presynaptic enhancement

To determine whether thiorphan-induced presynaptic potentiation was attributable to the activity of endogenously released Aβ or other neprilysin substrates, we examined its effects in cultures with reduced Aβ content (**Fig. 2**). Several methods have been used to reduce [Aβ]: hippocampal cultures lacking Aβ precursor protein (APP) produced from APP knockout[30] ($App^{-/-}$) mice; chelation of extracellular Aβ by specific 4G8 or HJ5.1 (ref. 8) monoclonal antibodies that recognize the intermediate Aβ domain; and reduction of Aβ production by inhibition of β- or γ-secretases. We first tested whether thiorphan affects presynaptic function in $App^{-/-}$ hippocampal cultures[30]. Thiorphan was ineffective in increasing either ΔF or D in neurons lacking APP ($n = 8$, $P > 0.6$; **Fig. 2a**,**c**,**d**). However, transient expression of human APP_{695} fused to YFP fluorophore (App^{YFP}) restored the thiorphan effect in $App^{-/-}$ hippocampal cultures ($n = 7$, **Fig. 2b–d**). We used FM4-64 to test the effect of thiorphan on presynaptic activity in APP^{YFP}-expressing neurons (**Fig. 2b**) compared with neurons expressing YFP only (**Fig. 2a**). Single synapse (**Fig. 2c**) and population (**Fig. 2d**) analysis revealed that thiorphan induced a four-fold increase in presynaptic strength at boutons expressing APP^{YFP} ($P < 0.001$), but did not produce presynaptic enhancement at non-transfected $App^{-/-}$ boutons ($P > 0.5$) or in boutons expressing YFP-only ($P > 0.3$, **Fig. 2c**,**d**). Interestingly, thiorphan also triggered three-fold potentiation in non-transfected $App^{-/-}$ boutons in the vicinity (≤50 μm) of APP^{YFP}-expressing dendrites ($n = 7$, $P < 0.001$, **Fig. 2c**,**d**). These data indicate that human Aβ might be released from either a pre- or post-synaptic compartment and can enhance presynaptic strength in a cell-autonomous fashion[6].

To further examine whether Aβ, a proteolytic derivative of APP, mediates thiorphan-induced presynaptic enhancement, we tested the ability of 4G8 antibody to prevent the effect of thiorphan. Incubation of hippocampal cultures with 4G8 (5 μg ml^{-1}, 1 h) reduced $[A\beta_{40}]_o$ and $[A\beta_{42}]_o$ by more than 80% ($n = 4$, $P < 0.001$, **Fig. 2e**) and prevented thiorphan from inducing an increase in presynaptic strength (**Fig. 2f–i**). Analysis of 224 FM^+ boutons revealed that thiorphan could not increase presynaptic strength in 4G8-pretreated neurons (**Fig. 2g**,**h**). On average ($n = 15$), neither ΔF nor D was changed following thiorphan application in 4G8-treated neurons ($P > 0.5$, **Fig. 2i**). Thiorphan-induced presynaptic potentiation was also precluded by the use of another Aβ monoclonal antibody, HJ5.1, to reduce $[A\beta]_o$ ($n = 6$, $P > 0.2$, **Fig. 2i**). Heat-denatured 4G8 and HJ5.1 antibodies (5 μg ml^{-1}, 1 h) failed to prevent the effect of thiorphan, confirming the molecular specificity of these antibodies in rescuing release probability ($n = 4$, $P < 0.001$ compared to control; **Fig. 2i**). To verify that Aβ mediates APP-dependent, thiorphan-induced presynaptic enhancement, we inhibited Aβ production using specific blockers of β-secretase (BACE1 inhibitor IV, 500 nM) or γ-secretase (L-685,458, 200 nM) ($n = 4$, $P < 0.0001$; **Fig. 2e**). Thiorphan had no effect on synaptic vesicle turnover in neurons with inhibited Aβ production ($n = 13$–16, $P > 0.2$; **Fig. 2i**). These results indicate that endogenous Aβ positively regulates the presynaptic strength of hippocampal synapses.

Inhibition of Aβ degradation increases mEPSC frequency

To test whether a thiorphan-induced increase in $[A\beta]_o$ affects quantal synaptic transmission, we measured miniature vesicle release in the presence of tetrodotoxin (TTX) at the level of presynaptic terminals using FM1-43 dye, and at the level of miniature AMPAR-mediated miniature excitatory postsynaptic currents (mEPSCs) using whole-cell voltage-clamp recordings. Analysis of the mEPSC recordings before and 10 min after thiorphan application (**Fig. 3a–c**) revealed an increase of 172 ± 28% in mEPSC frequency ($n = 11$, $P < 0.01$), but no change in mEPSC amplitude ($n = 11$, $P > 0.1$). No correlation was detected between series resistance and mEPSC frequency ($r^2 = 0.0002$, Pearson's correlation test, **Supplementary Fig. 6**), confirming that the differences across conditions are not attributable to variability in the quality of the recordings. Analysis of miniature vesicle recycling detected by FM1-43 under non-spike conditions

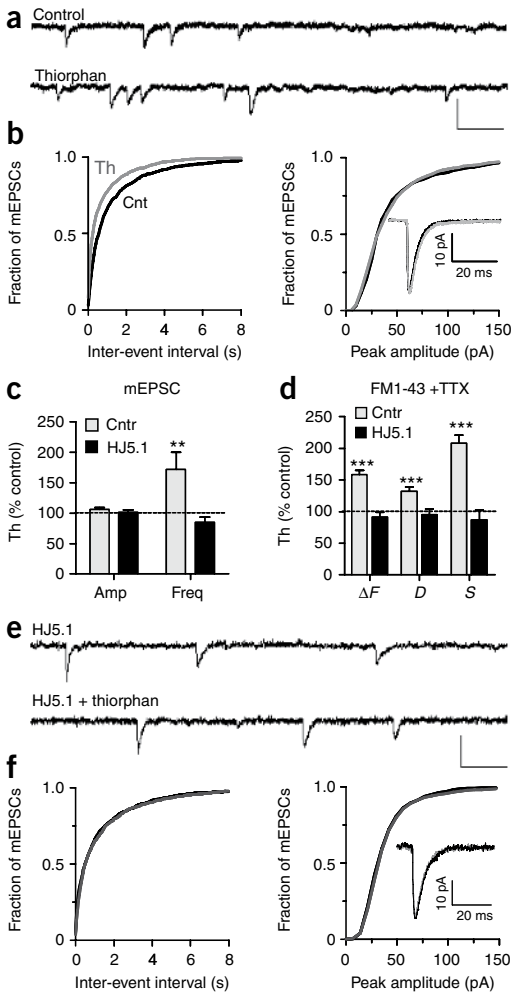

Figure 3 Inhibition of Aβ degradation increases miniature synaptic vesicle release and mEPSC frequency. Effect of thiorphan (500 nM, 10 min) in control (**a**,**b**) and HJ5.1-treated cultures (**e**,**f**). (**a**) Representative mEPSCs before (control) and after thiorphan application. (**b**) Cumulative distributions of the inter-event intervals (left) and mEPSC peak amplitude (right) before (black) and after (gray) thiorphan application. Differences between the conditions for the displayed mEPSC inter-event interval cumulative distributions are statistically significant ($P = 0.003$, K-S test). Differences between mEPSC amplitude distributions ($P = 0.1$, K-S test) are not significant. (**c**) Average effects of thiorphan on the frequency and peal amplitude of mEPSCs in control ($n = 11$) and HJ5.1-treated ($n = 9$) cultures. Thiorphan increased mEPSC frequency only in control cultures ($P < 0.01$). (**d**) Average effect of thiorphan on miniature vesicle recycling measured by FM1-43 in the presence of TTX (loading for 90 s without external stimulation). Thiorphan increased the total presynaptic strength of miniature vesicle exocytosis by 208 ± 13% ($n = 11$, $P < 0.001$) in control, but not in HJ5.1-treated ($n = 5$, $P > 0.3$) cultures. (**e**) Representative recordings of mEPSCs before and after thiorphan application in HJ5.1-treated (5 μg ml^{-1}, 2 h) cultures. (**f**) Cumulative distributions of the inter-event intervals (left) and mEPSC peak amplitudes (right) before (black) and after (gray) thiorphan application in HJ5.1-treated cultures. No statistical difference has been found between mEPSC amplitude ($P = 0.6$, K-S test) or inter-event interval ($P = 0.5$, K-S test) distributions. Error bars represent ± s.e.m. Scale bars: 40 pA, 64 ms (**a**,**e**). * $P < 0.05$, ** $P < 0.01$, *** $P < 0.001$.

revealed a significant increase in presynaptic strength by 208 ± 13% ($n = 11$, $P < 0.0001$; **Fig. 3d**) after acute thiorphan application.

To test whether the thiorphan-induced increase in mEPSC frequency is mediated by Aβ peptides, we repeated the experiments described above in cultures pretreated with anti-Aβ antibodies. In HJ5.1-treated cultures, thiorphan affected neither the frequency nor the amplitude of mEPSCs ($n = 9$, $P > 0.5$; **Fig. 3c–f**), and nor did it affect miniature vesicle recycling ($n = 5$, $P > 0.3$; **Fig. 3d**). These results suggest that on a rapid timescale, endogenously released Aβ peptides enhance the probability of quantal transmitter release, without altering the number of postsynaptic AMPA receptors.

Aβ-mediated presynaptic enhancement is history dependent

Having established a positive relationship between $[A\beta]_o$ and basal synaptic vesicle release, we investigated how inhibition of Aβ degradation affects vesicle release and synaptic transmission evoked by high-frequency discharges. Given the inverse relationship between release probability and paired-pulse facilitation[31,32], Aβ should trigger a reduction in short-term facilitation during periods of correlated activity. To test this prediction, we measured the total number of recycled synaptic vesicles stimulated by a constant number of spikes (30 action potentials) at various frequencies and temporal patterns. The following stimulation parameters were modified: frequency of spikes; temporal pattern (continuous versus burst); and inter-burst interval. To prevent the induction of long-term plasticity by bursts, we applied a postsynaptic glutamate receptor blocker (kynurenic acid).

First, we assessed the effect of thiorphan on vesicle recycling triggered by spikes at gradually increasing rates (10–100 Hz). The magnitude of thiorphan-induced presynaptic potentiation was inversely proportional to stimulation frequency: it was ~35% lower at 10 Hz than at 1 Hz, and was completely abolished at higher frequencies of ≥50 Hz (**Fig. 4a**,**b**). Furthermore, the temporal spike pattern affected the thiorphan-induced potentiation at intermediate stimulation frequencies of 10–20 Hz; the magnitude of potentiation was higher for continuous stimulation than for short bursts ($n = 7$–9, $P < 0.05$). However, at spike rates ≥50 Hz, thiorphan did not influence presynaptic activity for either pattern. Moreover, decreasing the inter-burst interval from 5 to 0.2 s did not enhance the susceptibility of vesicle recycling to thiorphan during 100-Hz bursts (**Fig. 4c**, $n = 9$–11, $P > 0.3$). These data cannot be explained by saturation of synaptic vesicle release or optical signal, as a similar reduction in the inter-burst interval under control conditions enhanced the average fluorescence intensity of boutons (**Supplementary Fig. 7**).

Finally, we assessed the effect of thiorphan on 'natural' stimulation patterns derived from CA1 hippocampal place-cell firing in freely moving rats (the sequence was provided by A. Lee and M. Wilson, unpublished data). Periods of high-frequency discharges from two CA1 cells with a mean inter-spike interval of 46 ± 3 ms (3–237 ms) corresponding to the cell's place field were selected as stimulation patterns (**Fig. 4d**). Thiorphan induced a small presynaptic enhancement during 'natural' high-frequency discharges (126 ± 5% for *S*, $n = 11$, $P < 0.01$, 4 epochs from 2 cells; **Fig. 4e**). Together, these data suggest that there is an inverse relationship between spike frequency and the magnitude of Aβ-mediated presynaptic effects with some contribution of the temporal spike pattern at intermediate firing rates.

The above analysis of synaptic vesicle recycling enables us to estimate presynaptic activity at the single synapse and network levels, but lacks high temporal (millisecond) resolution. To investigate the effect of thiorphan on the input/output relationship for bursts, we measured evoked AMPAR-mediated EPSCs between pairs of excitatory neurons, using a double-perforated patch-clamp technique to preserve the intracellular environment of neurons. Bursts were evoked in presynaptic neurons held in the current-clamp mode, whereas the EPSCs from postsynaptic neurons were recorded at

© 2009 Nature America, Inc. All rights reserved.

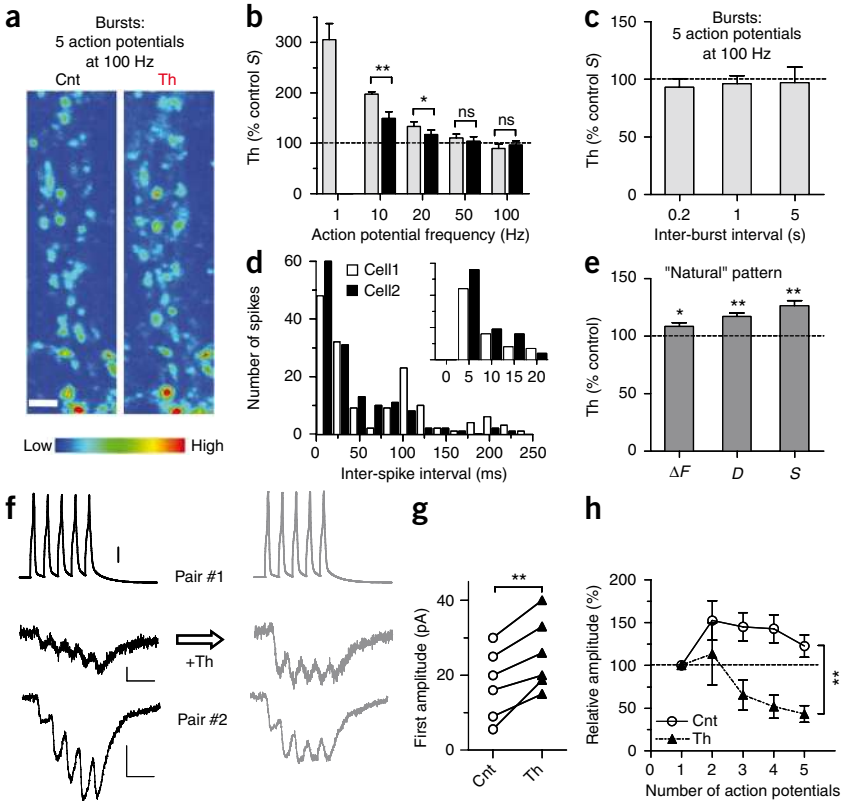

Figure 4 Potentiation of vesicle release by thiorphan depends on the history of synaptic activation. (**a**) Representative ΔF images before and after application of thiorphan stained during stimulation by bursts (30 action potentials in 6 bursts; each burst contains 5 action potentials; inter-spike interval, 10 ms). Scale bar: 2 μm. (**b**) Average effect of thiorphan ($n = 6$–9) on *S* for two stimulation patterns with varying (1–100 Hz) frequencies: (i) 30 action potentials delivered continuously at a given frequency (gray bars); (ii) 30 action potentials distributed in 6 bursts (inter-burst interval, 5 s; black bars). (**c**) Average effect of thiorphan on *S* for 30 action potentials distributed in 6 bursts with varying inter-burst intervals (0.2–5 s), but constant inter-spike interval of 10 ms ($n = 9$–11, $P > 0.3$). (**d**) Inter-spike interval histogram for 'natural' stimulation pattern (A. Lee and M. Wilson, unpublished data) used for the experiments presented in **e**. Insert: magnification of small inter-spike-intervals. (**e**) Average effect of thiorphan on presynaptic strength for 30 action potentials delivered in 'natural' patterns ($n = 11$, $P < 0.01$ for *S*). (**f**) Examples of the effect of thiorphan on synaptic currents in two pairs of neuronal connections. (**g**) Effect of thiorphan on the first EPSC amplitude in the burst ($n = 6$, $P < 0.01$). (**h**) Averaged relative amplitudes of EPSCs within the burst, normalized to the first peak. Thiorphan increased synaptic depression during the burst ($n = 6$, $P < 0.01$). Error bars represent ± s.e.m. * $P < 0.05$, ** $P < 0.01$, *** $P < 0.001$.

a holding potential of −70 mV. As shown in the representative recordings depicted in **Figure 4f**, acute thiorphan application resulted in an increase in amplitude of the first EPSC within the burst, but its effect on the amplitude of the last EPSC varied from no change (pair 1; **Fig. 4f**) to a decrease (pair 2; **Fig. 4f**). On average ($n = 6$), thiorphan increased the first EPSC amplitude by 171 ± 33% ($P < 0.01$; **Fig. 4g**), without a significant change in the integrated burst charge transfer ($P > 0.1$). Consequently, thiorphan decreased short-term synaptic facilitation and/or increased short-term depression in excitatory synaptic connections, as estimated by the reduction in the relative EPSC amplitude within the burst ($P < 0.01$; **Fig. 4h**). These results suggest that inhibition of Aβ degradation induces history-dependent enhancement of synaptic transmission, converting excitatory synaptic connections into low-pass filters.

Aβ positively regulates ongoing neuronal activity

To assess the effect of an Aβ-mediated increase in release probability on ongoing neuronal activity, we recorded the spontaneous neuronal firing rate using perforated whole-cell current-clamp (**Fig. 5a**), and imaged spontaneous vesicle exocytosis in the absence of external stimulation

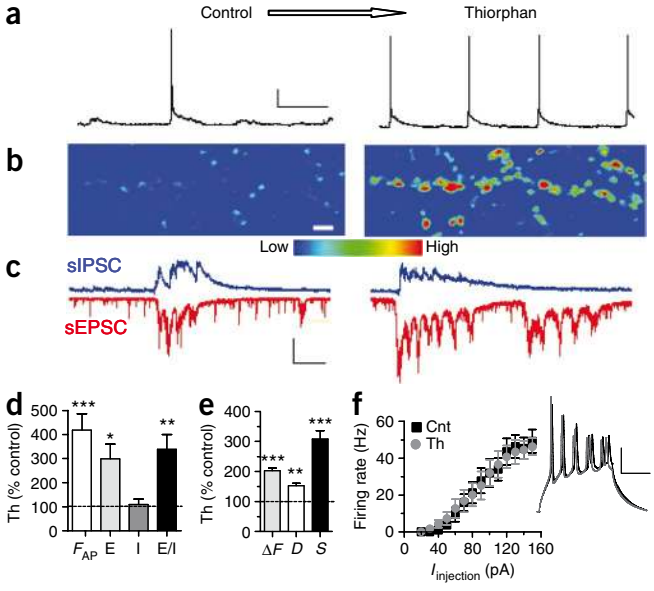

Figure 5 Inhibition of Aβ degradation increases ongoing spontaneous activity through a shift in E/I balance. (**a**) Representative recordings of spontaneous firing of pyramidal hippocampal neurons before and after thiorphan application. Neurons were kept in current-clamp mode. Scale bars: 20 mV, 3 s. (**b**) Effect of thiorphan on spontaneous vesicle recycling measured by FM1-43 (loading for 90 s without external stimulation). Scale bar: 2 μm. (**c**) Effects of thiorphan on sEPSC and sIPSC at the level of single pyramidal neurons. Scale bars: 300 pA, 5 s. Neurons were held sequentially at −70 mV (reversal potential for $GABA_A$R-mediated currents) to isolate sEPSCs and at +4 mV (reversal potential for AMPAR-mediated currents) to isolate sIPSCs. (**d**) Average effect of thiorphan on mean firing rate (F_{AP}: $n = 14$, $P < 0.0001$), sEPSC charge transfer (E: $n = 6$, $P < 0.05$), sIPSC charge transfer (I: $n = 6$, $P > 0.4$), and E/I balance (E/I: $n = 6$, $P < 0.01$). (**e**) Average effect of thiorphan on spontaneous vesicle recycling ($n = 12$, $P < 0.0001$ for *S*). (**f**) Frequency-current relationship before and after thiorphan application ($n = 9$). *Right*, current clamp recordings for the injected DC current (100 ms, 120 pA) before (black line) and after (gray line) thiorphan application. Scale bars: 20 mV, 40 ms. In all the experiments (**a**–**f**) the effect of thiorphan (500 nM) was quantified 10 min after its application. Error bars represent ± s.e.m. * $P < 0.05$, ** $P < 0.01$, *** $P < 0.001$.

© 2009 Nature America, Inc. All rights reserved.

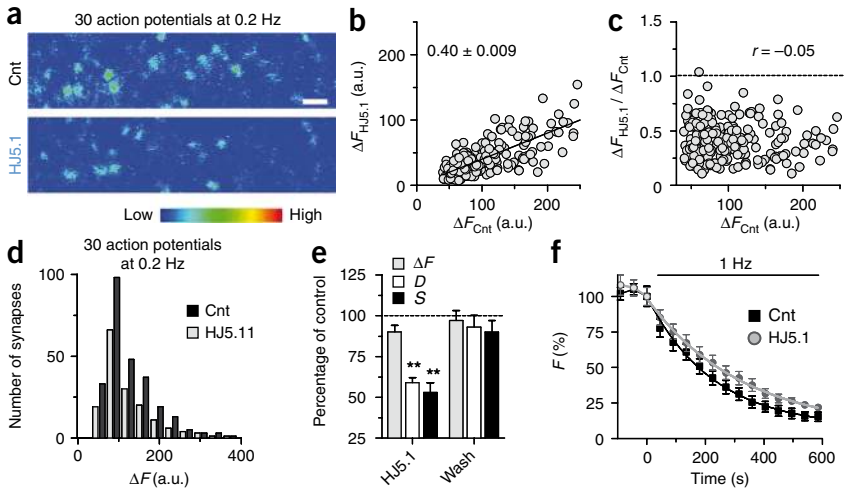

Figure 6 Neutralization of $[A\beta]_o$ reduces presynaptic activity of hippocampal synapses. (**a**) Representative high-magnification ΔF images obtained before and 30 min after application of HJ5.1 antibody (5 μg ml^{-1}). Stimulation during FM1-43 staining: 30 action potentials at 0.2 Hz. Scale bar: 2 μm. (**b**) Effect of HJ5.1 at the level of single synapses. Slope of linear fit is 0.4 ± 0.01 (for 240 synapses). (**c**) HJ5.1-induced presynaptic inhibition does not depend on the initial presynaptic strength (the same data as in **b**, Spearman $r = -0.06$, $P > 0.3$). (**d**) Histograms of ΔF before (black bars) and after (gray bars) HJ5.1 application in a single experiment. The median ΔF decreased from 102 to 94 arbitrary units (a.u.), and the number of FM$^+$ boutons decreased from 267 to 173. (**e**) Average effect of HJ5.1 on presynaptic strength across population of synapses ($n = 6$, $P < 0.01$) was reversible upon 30 min of washout ($n = 4$). (**f**) Effect of HJ5.1 on the destaining rate of 264 synapses during 1 Hz stimulation. Destaining rate constants were 0.0044 ± 5 × 10^{-5} and 0.0031 ± 9 × 10^{-6} s^{-1} in control and HJ5.1, respectively. Error bars represent ± s.e.m. * $P < 0.05$, ** $P < 0.01$, *** $P < 0.001$.

using FM1-43 (**Fig. 5**). Thiorphan application significantly increased the neuronal firing rate by 418 ± 68% from 0.5 ± 0.15 to 2.1 ± 0.4 Hz ($n = 14$, $P < 0.001$; **Fig. 5**) and spontaneous vesicle exocytosis by 308 ± 28% ($n = 12$, $P < 0.0001$; **Fig. 5e**). The observed increase in spontaneous firing rate could be achieved by shifting E/I balance or by increasing the intrinsic excitability of neurons. To assess the effect of thiorphan on E/I balance directly, we isolated the spontaneous excitatory and inhibitory postsynaptic currents (sEPSC and sIPSC, respectively; **Fig. 5c**) at the same cell, based on the reversal potentials of AMPAR- and $GABA_A$R-mediated currents, respectively. We found that thiorphan increased the sEPSC charge transfer (from 21 ± 4 to 59 ± 15 nC, $n = 10$, $P < 0.05$,) without significantly altering the sIPSC charge transfer (51 ± 13 versus 53 ± 15 nC, $n = 10$, $P > 0.7$), resulting in an increase of 339 ± 61% in E/I ratio (0.52 ± 0.07 versus 1.6 ± 0.3, $n = 10$, $P < 0.01$; **Fig. 5d**). In the HJ5.1-treated cultures, thiorphan did not affect either sEPSC or sIPSC charge transfer ($n = 9$, $P > 0.2$, **Supplementary Fig. 8**), and subsequently did not change the E/I ratio ($n = 9$, $P > 0.7$, **Supplementary Fig. 8**), suggesting that the thiorphan-induced increase in excitatory drive is mediated by extracellular Aβ peptides.

To assess the effect of thiorphan on the intrinsic excitability of neurons, we measured the frequency of action potential firing in response to different levels of depolarizing current injection (FI curve) in the presence of synaptic transmission blockers. On average ($n = 9$), there was no significant change in the FI curve after acute thiorphan application ($P > 0.1$; **Fig. 5f**). Neither the threshold current for action potential generation (69.8 ± 7.9 versus 73.7 ± 8.6 pA, $P > 0.6$), nor the maximal action potential rate (49.3 ± 6.5 versus 46.3 ± 4.5, $P > 0.2$) was affected by thiorphan. Input resistance (237.8 ± 24.4 versus 242.6 ± 26.2 MΩ, $P > 0.6$) and resting membrane potential (−71.4 ± 1.0 versus −71.7 ± 1.3 mV, $P > 0.4$) were not significantly altered. These data suggest that inhibition

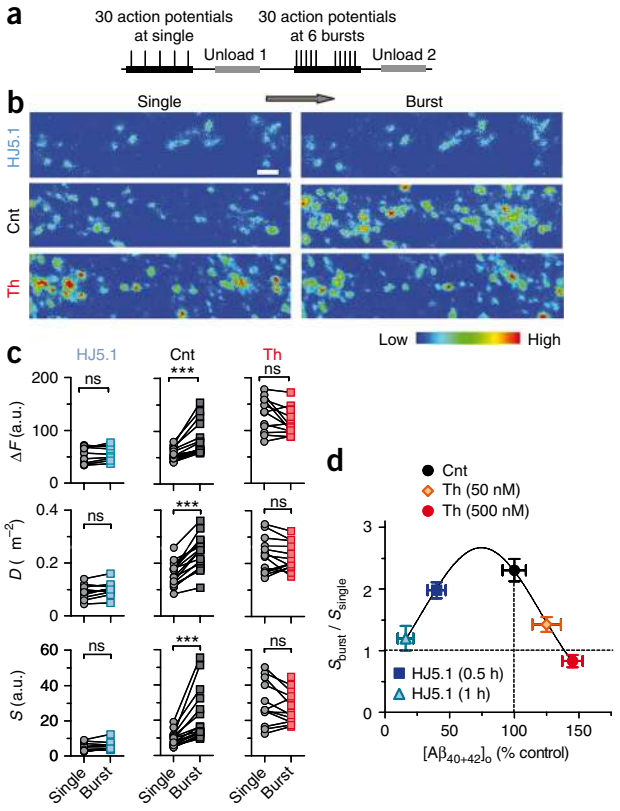

Figure 7 Optimal $[A\beta]_o$ enables maximal short-term presynaptic facilitation by bursts. (**a**) Experimental protocol used to determine short-term plasticity indexed through S_{burst}/S_{single} (S_{single}: 30 action potentials at 0.2 Hz; S_{burst}: 30 action potentials in 6 bursts, where each burst contained 5 action potentials; inter-spike interval, 10 ms; inter-burst interval, 5 s). (**b**) Representative high-magnification ΔF images for single and burst stimulations under control conditions ($[Ca^{2+}]_o/[Mg^{2+}]_o = 1$), in the presence of thiorphan (500 nM), and in the presence of HJ5.1 (5 μg ml^{-1}, 1 h). Scale bar: 2 μm. (**c**) ΔF, D and S for single versus burst inputs over synapse population in control ($n = 16$, $P < 0.0001$), thiorphan-treated ($n = 13$) and HJ5.1-treated ($n = 10$) cultures. (**d**) The magnitude of short-term plasticity as a function of $[A\beta_{40+42}]_o$. S_{burst}/S_{single} under control conditions ($n = 16$, black symbols); following reduction in $[A\beta_{40+42}]_o$ by 65 ± 4% (HJ5.1, 5 μg ml^{-1}, 30 min; $n = 4$, $P < 0.001$, light blue symbol) and by 86 ± 4% (HJ5.1, 5 μg ml^{-1}, 1 h; $n = 4$, $P < 0.001$, dark blue symbol); after a thiorphan-induced increase in $[A\beta_{40+42}]_o$ by 125 ± 15% (50 nM thiorphan; $n = 3$, $P < 0.001$, orange symbol) and by 145 ± 8% (500 nM thiorphan; $n = 4$, $P < 0.001$, red symbol). Error bars represent ± s.e.m. * $P < 0.05$, ** $P < 0.01$, *** $P < 0.001$.

© 2009 Nature America, Inc. All rights reserved.

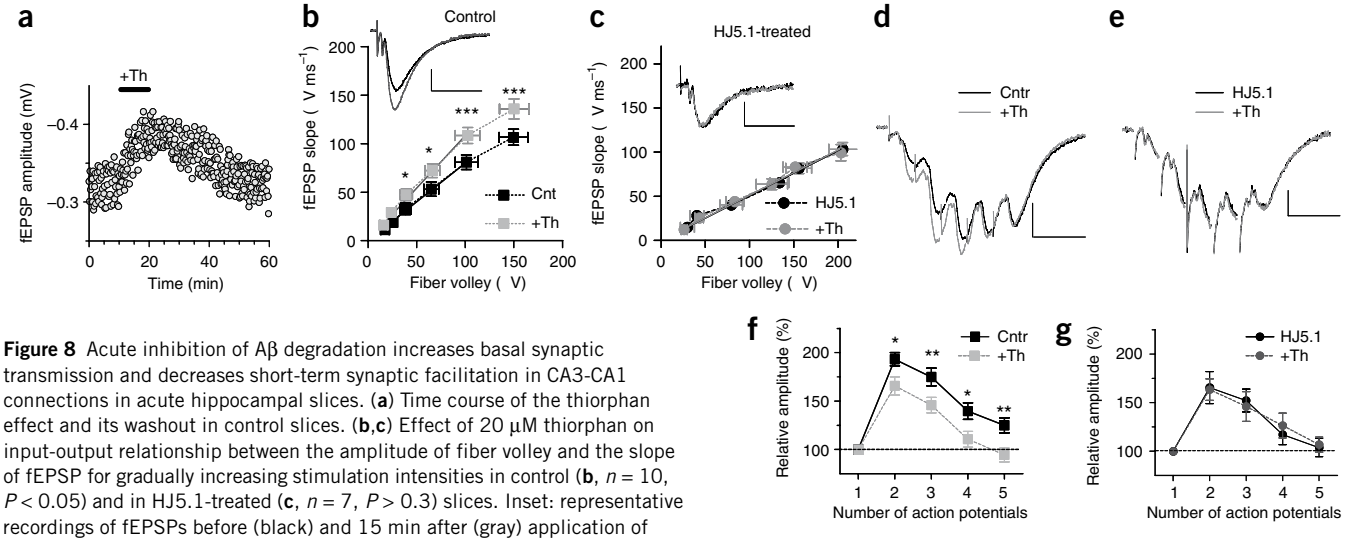

Figure 8 Acute inhibition of Aβ degradation increases basal synaptic transmission and decreases short-term synaptic facilitation in CA3-CA1 connections in acute hippocampal slices. (**a**) Time course of the thiorphan effect and its washout in control slices. (**b**,**c**) Effect of 20 μM thiorphan on input-output relationship between the amplitude of fiber volley and the slope of fEPSP for gradually increasing stimulation intensities in control (**b**, $n = 10$, $P < 0.05$) and in HJ5.1-treated (**c**, $n = 7$, $P > 0.3$) slices. Inset: representative recordings of fEPSPs before (black) and 15 min after (gray) application of thiorphan. Scale bars: **b**, 0.2 mV, 20 ms; **c**, 0.1 mV, 20 ms. (**d**,**e**) Representative recordings of fEPSPs evoked by a burst (each burst contains 5 action potentials; inter-spike interval, 10 ms; inter-burst interval, 30 s) before (black) and 15 min after (gray) application of thiorphan in control (**d**, scale bars: 0.2 mV, 20 ms) and in HJ5.1-treated (**e**, scale bars: 0.1 mV, 20 ms) slices. (**f**,**g**) Average relative amplitudes of fEPSPs within the burst, normalized to the first peak. Thiorphan reduced synaptic facilitation during the burst in control (**f**, $n = 6$, $P < 0.01$), but had no effect in HJ5.1-treated slices (**g**, $n = 6$, $P > 0.8$). Error bars represent ± s.e.m. * $P < 0.05$, ** $P < 0.01$, *** $P < 0.001$.

of Aβ degradation results in over-excitation of the hippocampal network through an increase in the E/I ratio.

Endogenous Aβ maintains basal presynaptic activity

To assess the involvement of $[A\beta]_o$ in tonic regulation of release probability, we tested the effects of the HJ5.1 antibody on basal presynaptic activity (**Fig. 6a**). Single synapse analysis revealed that a reduction in $[A\beta]_o$ (5 μg ml^{-1} HJ5.1, 1 h) induced a ~60% decrease in ΔF values across the boutons (**Fig. 6b**). No correlation was detected between initial ΔF and the degree of presynaptic inhibition (Spearman $r = -0.05$, $P > 0.4$; **Fig. 6c**). Population synapse analysis of the effect of HJ5.1 revealed a decrease in presynaptic activity mainly through reduction in the density of FM$^+$ puncta (**Fig. 6d**,**e**). On average, treatment with HJ5.1 reduced presynaptic strength to 53 ± 6% of control ($n = 6$, $P < 0.01$; **Fig. 6e**). This presynaptic suppression was reversible upon 30 min washout of the antibody ($n = 4$; **Fig. 6e**). To confirm that a reduction in $[A\beta]_o$ below normal levels suppresses synaptic vesicle exocytosis, we tested the effect of the HJ5.1 antibody on the rate of FM1-43 destaining induced by 1-Hz stimulation. Chelation of Aβ by HJ5.1 caused a 30% decrease in the destaining rate constant (264 synapses, $n = 3$, $P < 0.001$; **Fig. 6f**). In addition, a decrease in presynaptic strength was detected following a reduction in Aβ production (0.5 μM BACE1-inhibitor IV, S = 48 ± 6% of control, $n = 20$, $P < 0.0001$; 0.2 μM L-685,458, S = 49 ± 3% of control, $n = 13$, $P < 0.001$). These results suggest that extracellular Aβ might be involved in the maintenance of basal synaptic vesicle release in hippocampal synapses.

Optimal $[A\beta]_o$ enables maximal presynaptic facilitation

Although our results indicate that an increase in $[A\beta]_o$ reduces short-term presynaptic facilitation, it is still unclear whether facilitation monotonically relates to $[A\beta]_o$. To address this issue, we determined the magnitude of presynaptic facilitation during bursts over a wide range of $[A\beta]_o$ (**Fig. 7**). The magnitude and the sign of short-term presynaptic plasticity (S_{burst}/S_{single}) was calculated by dividing the total number of vesicles recycled in response to bursts by the number of vesicles recycled by a similar number of single spikes in the same population of synapses (**Fig. 7a**). $S_{burst}/S_{single} > 1$ reflects short-term facilitation, whereas $S_{burst}/S_{single} < 1$ reflects short-term depression. On average, hippocampal synapses exhibited 2.3 ± 0.2 facilitation over the synaptic population at a physiological $[Ca]_o/[Mg]_o$ ratio (1.2/1.2 mM; $n = 16$, $P < 0.0001$; **Fig. 7b–d**), displaying stronger facilitation at low-*P*r synapses ($n = 4$, Spearman $r = -0.67$, $P < 0.0001$; **Supplementary Fig. 9**). Strikingly, facilitation of vesicle release was attenuated at both increased and reduced $[A\beta]_o$ (**Fig. 7b–d**). Increasing $[A\beta_{40+42}]_o$ by ~25% (thiorphan, 50 nM) resulted in a decrease of synaptic facilitation to 1.4 ± 0.1 ($n = 5$, $P < 0.01$; **Fig. 7d**), whereas further boosting $[A\beta_{40+42}]_o$ by ~45% (thiorphan, 500 nM) completely abolished synaptic facilitation (0.9 ± 0.07, $n = 13$, $P < 0.0001$; **Fig. 7c**,**d**) due to an increase in release probability (**Fig. 1**). On the other hand, reducing $[A\beta_{40}+_{42}]_o$ by ~60% (5 μg ml^{-1} HJ5.1, 0.5 h) triggered a slight decrease in presynaptic facilitation compared to control (2.0 ± 0.1, $n = 5$; $P < 0.05$; **Fig. 7d**), whereas further reduction in $[A\beta_{40}+_{42}]_o$ by ~86% (5 μg ml^{-1} HJ5.1, 1 h) resulted in a marked decrease in S_{burst}/S_{single} (1.2 ± 0.07, $n = 10$, $P < 0.001$; **Fig. 7c**,**d**). An increase in $[Ca^{2+}]_o$ rescued S_{burst}/S_{single} in HJ5.1-treated cultures (**Supplementary Fig. 9**), suggesting that Ca^{2+}-dependent mechanisms underlie the decrease in presynaptic facilitation produced by Aβ chelation. In addition, a substantial reduction in short-term facilitation was detected when Aβ production was reduced by >90% (**Supplementary Fig. 9**). Together, our data suggest that there is a bell-shaped relationship between short-term facilitation of presynaptic terminals and $[A\beta]_o$, indicating that physiological Aβ levels keep hippocampal synapses in a high-pass filter mode.

Aβ regulates synaptic transmission in hippocampal slices

Finally, we investigated whether acute inhibition of Aβ degradation by thiorphan affects synaptic transmission in a more intact preparation; namely, in acute hippocampal slices (**Fig. 8**). Extracellularly recorded field EPSPs (fEPSPs) evoked by low frequency spikes (0.1 Hz) were used to assess the strength of basal synaptic transmission between hippocampal CA3 and CA1 cells (Schaffer collateral-commissural pathway). Acute application of thiorphan induced a reversible increase in fEPSP amplitude (**Fig. 8a**). On average, thiorphan increased the slope of the input (amplitude of

© 2009 Nature America, Inc. All rights reserved.

fiber volley)/output (slope of fEPSP) curve (I/O curve) by ~35% (from 0.8 ± 0.015 to 1.1 ± 0.026, $n = 10$, $P < 0.01$; **Fig. 8b**), pointing to an increase in basal synaptic transmission. To test whether an increase in the basal transmitter release could underlie the positive effect of thiorphan on fEPSPs, we measured its effect at a high $[Ca^{2+}]_o/[Mg^{2+}]_o$ ratio. Thiorphan failed to increase the fEPSP at high $[Ca^{2+}]_o/[Mg^{2+}]_o$ (3.6/1.2 mM, 101 ± 2%, $n = 7$, $P > 0.3$) compared to its effect at physiological concentration (1.2/1.2 mM; 145 ± 9%, $n = 7$, $P < 0.005$). Analysis of the effect of thiorphan on short-term synaptic plasticity during bursts revealed a significant increase in the peak amplitude of the first fEPSP within the burst, but no change in the last one (**Fig. 8d**,**f**). Thiorphan decreased the ratio of the last peak amplitude to the first peak amplitude by ~25% ($n = 6$, $P < 0.01$; **Fig. 8f**), suggesting a reduction in short-term facilitation due to an increase in basal transmitter release.

To determine whether the effect of thiorphan on CA3-CA1 synaptic transmission in acute hippocampal slice was attributable to the action of endogenously released Aβ, we tested the effect of thiorphan in slices pre-incubated with HJ5.1 antibody (5 μg ml^{-1}, 1 h). Chelation of $[A\beta]_o$ by HJ5.1 occluded the effect of thiorphan on the fiber volley/fEPSP relationship ($n = 7$, $P > 0.3$; **Fig. 8c**). Notably, the I/O slope was significantly reduced after pre-treatment with Aβ antibody (0.51 ± 0.01 versus 0.08 ± 0.015 in control, $P < 0.001$), suggesting a reduction in basal synaptic transmission after Aβ chelation. Moreover, pretreatment with HJ5.1 occluded the effect of thiorphan on burst-evoked synaptic transmission ($n = 6$, $P > 0.8$; **Fig. 8e**,**g**). These data confirm that endogenously released Aβ positively regulates basal synaptic transmission in a history-dependent manner, resulting in reduction of short-term facilitation by bursts in the CA3-CA1 pathway in acute hippocampal slices.

DISCUSSION

Extensive experimental efforts over the past decade have identified the effects of chronic elevation in [Aβ] on the synaptic 'failure' that precedes cognitive decline in transgenic mouse models of Alzheimer's disease[33]. However, the initial steps underlying the very early phases of synaptic dysfunction, as well as the physiological functions of Aβ, remain obscure. In this study we focused on identification of the primary, fast-timescale effects mediated by endogenous Aβ peptides on synaptic activity at the level of individual presynaptic terminals, neuronal connections and synaptic networks. Our results indicate that endogenously released Aβ peptides have a critical role in the regulation of synaptic transfer function under physiological and pathological conditions.

Aβ and synaptic transfer function

The dependency of synaptic transmission on spike pattern is a universal property of central and peripheral synapses[34,35]. Input/output relationships in synaptic connections show a high degree of heterogeneity and depend primarily on the basal release probability of synapses[34–36]. Interestingly, there is a rich repertoire of negative endogenous regulators of neurotransmitter release. Presynaptic G-protein-coupled receptors (GPCRs), such as the $GABA_B$, metabotropic glutamate, muscarinic, adenosine and cannabinoid receptors, typically mediate the feedback inhibition of basal neurotransmitter release. This diversity of negative endogenous regulatory pathways might make possible the marked synaptic plasticity in hippocampal networks.

Our results reveal that Aβ acts as a positive endogenous modulator of release probability in hippocampal synapses. The acute effects induced by endogenous Aβ peptides in our studies were exclusively presynaptic, without any detectable change in postsynaptic function or intrinsic neuronal excitability. The enhancement of release probability by Aβ was non-uniform, and negatively correlated to basal presynaptic strength, suggesting that 'unreliable' low-*P*r terminals might be more susceptible to $[A\beta]_o$ fluctuations. The electrophysiological data indicate that excitatory synapses are highly sensitive to changes in Aβ levels, whereas inhibitory drive remained relatively immune to immediate effects of Aβ. However, future studies are required to determine whether Aβ differentially affects excitatory-excitatory, excitatory-inhibitory, inhibitory-inhibitory, and inhibitory-excitatory synaptic connections.

Aβ-mediated presynaptic potentiation, like GPCR-mediated presynaptic inhibition, depends on the history of synaptic activation, reducing its impact at higher firing rates. Several mechanisms might underlie this frequency-dependent phenomenon. First, it might stem from a decrease in Aβ release during high-frequency stimulation. However, $[A\beta]_o$ positively correlates to the level of neuronal activity in APP-transgenic[6,7] and wild-type[8] mice, making this unlikely. Alternatively, the inability of thiorphan to increase presynaptic activity during bursts with long inter-burst intervals might be explained by the short life-time of Aβ in the synaptic cleft. Nevertheless, thiorphan effectively enhanced presynaptic activity for single spikes with inter-spike intervals equal to the applied inter-burst intervals (**Fig. 4b**,**c**). Therefore, a reduction in the responsiveness of presynaptic terminals to Aβ during bursts seems to be the most plausible explanation for the observed phenomenon. Further studies should be conducted to identify the molecular mechanism involved in frequency-dependent enhancement of synaptic vesicle release by endogenous Aβ.

An intriguing finding in this study was that short-term synaptic facilitation, a mechanism that is thought to be involved in information processing and memory function[37], was impaired not only at increased but also at significantly (>60%) decreased $[A\beta]_o$ (**Fig. 7d**). Although a reduction in synaptic facilitation at increased $[A\beta]_o$ might simply occur due to a greater probability of vesicle release, as suggested by the residual calcium hypothesis[34,38], a decrease in facilitation at lowered $[A\beta]_o$ could be attributed to the reduced size of the readily releasable pool of vesicles[27,32] or reduced Ca^{2+} cooperativity in triggering vesicle fusion[39]. Regardless of the precise molecular mechanism, Aβ peptides might maintain release probability in the optimal range, enabling the efficient transfer of temporospatially correlated inputs in hippocampal networks.

Rodent Aβ, which differs from human Aβ at three amino acids, is less susceptible to oligomerization. Therefore, it was essential to examine the effects of human endogenously released Aβ on presynaptic strength. Thiorphan triggered a pronounced enhancement of vesicle recycling in neurons expressing APP^{YFP} in $App^{-/-}$ cultures, indicating that the presynaptic effects of Aβ do not depend on the primary peptide structure. Presynaptic potentiation was also observed for two main human Aβ isoforms, $Aβ_{1\text{-}40}$ and $Aβ_{1\text{-}42}$ (**Supplementary Fig. 5**). However, the effective concentrations of ectopically applied synthetic peptides were several orders of magnitude higher than the steady-state endogenous $[A\beta]_o$ elevated by neprilysin inhibition, thus seriously impeding the interpretation of these results. Therefore, at this stage, we were unable to identify the isoforms and conformations of the endogenously released Aβ peptides that induce presynaptic enhancement.

Although the impairment of synaptic and cognitive functions in Alzheimer's disease is widely believed to be triggered by the rise in [Aβ], the relationship between reduced Aβ levels and synaptic state is less clear. Impaired synaptic plasticity, spatial learning and memory have been observed in $App^{-/-}$ (refs. 40,41), $BACE1^{-/-}$ (ref. 42) and *PS1/PS2* conditional knockout[43] mice. Furthermore, the injection of small amounts of $Aβ_{42}$ can enhance long-term synaptic potentiation and memory, in contrast to the synaptic impairments produced by

© 2009 Nature America, Inc. All rights reserved.

injection of high $A\beta_{42}$ concentrations[44]. The bell-shaped relationship between $[A\beta]_o$ and synaptic plasticity might have several clinical implications. For example, boosting of ongoing neuronal activity induced by inhibition of Aβ degradation might have potential significance for epileptic activity in the early stages of Alzheimer's disease[45]. Furthermore, various pathological conditions associated with the reduction in neuronal activity might lead to decrease in $[A\beta]_o$ and, consequently, impairment of synaptic transmission capability. A recent study in human subjects with acute brain injury provided the first evidence of a correlation between the amount of Aβ in brain interstitial fluid and neurological status[46]. Finally, the fact that a reduction in $[A\beta]_o$ decreases synaptic facilitation should be taken into account when developing potential therapies for Alzheimer's disease based on inhibition of Aβ production or neutralization of Aβ.

Aβ and synaptic homeostasis

Synaptic loss is the best-known correlate of cognitive decline in Alzheimer's disease patients[14]. Therefore, identification of the cellular mechanisms that trigger the reduction in synapse number is of critical importance. Previous studies have shown that downregulation in the density and strength of APP-overexpressing synapses occurs slowly, over months *in vivo*[47] and days *in vitro*[15]. Such time courses are typical of the expression of homeostatic and metaplastic changes in a wide range of synapses. The question then arises: what are the primary versus compensatory changes induced by an increase in $[A\beta]_o$?

Having established a negative relationship between Aβ degradation and ongoing neuronal activity on a rapid timescale, we examined whether long-term inhibition of Aβ degradation triggers a reduction in the number of functional presynaptic terminals. Hippocampal cultures were pre-incubated with thiorphan for 48 h, and the density of functional synaptic terminals capable of vesicle recycling was determined by a maximal stimulation protocol (600 action potentials at 20 Hz). The number of FM^+ functional synapses obtained by this protocol correlates highly with structural findings[28]. Our data demonstrated a reduction in the density of functional terminals, accompanied by an increase in the area of the fluorescent puncta after prolonged thiorphan application (**Supplementary Fig. 10**). These results are important for several reasons. They show that long-term inhibition of Aβ degradation leads to synaptic loss, similar to APP overexpression[15,16,47]. Second, they demonstrate that accumulation of rodent Aβ, displaying a different primary structure and lower amyloidogenic potential than human Aβ, triggers a loss of presynaptic terminals, a prominent feature of the brains of patients with Alzheimer's disease[13,14]. Third, the data suggest that the loss of functional terminals triggers a compensatory increase in the area of the remaining active terminals, similar to the compensatory increase in postsynaptic density size in patients with Alzheimer's disease[48]. Finally, they provide evidence that thiorphan-sensitive Aβ-degrading peptidases, such as neprilysin, might be critical for regulating synaptic density. The increase in neuronal activity triggered by the deficit in Aβ degradation might represent the first step in a cascade that leads to a compensatory reduction in the number of synapses to balance the ongoing activity of the hippocampal network. Given that Aβ overproduction has been implicated in less than 1% of the cases of Alzheimer's disease, a deficit in Aβ clearance might contribute to the development of synaptic loss and memory decline in the most common cases (late-onset Alzheimer's disease)[9].

Together, the results of this study suggest that endogenously released Aβ peptides are essential for maintaining synaptic vesicle release in a functional range, optimizing the high-pass filter properties of excitatory hippocampal synapses. Given the remarkable correlation between a high default brain activity in young adults and a spatial pattern of amyloid depositions in elderly individuals with Alzheimer's disease[49], it is worth examining whether an increase in ongoing neuronal activity and a decrease in synapse capacity for burst transfer might represent a basic feature of the crucial early pathological phase that leads to synapse loss in the common form of late-onset Alzheimer's disease.

METHODS

Methods and any associated references are available in the online version of the paper at http://www.nature.com/natureneuroscience/.

Note: Supplementary information is available on the Nature Neuroscience website.

ACKNOWLEDGMENTS

We thank A. Lee and M. Wilson for sharing unpublished data on 'natural' spike sequence, D.M. Holtzman for providing the HJ5.1 hybridoma cell line, A.I. Bush, R. Cappai and H. Zheng for *App*$^{-/-}$ mice, C. Kaether for the human APP_{695}-YFP cDNA construct, and the members of our laboratory for comments on the manuscript. We thank A.I. Bush and E. Gazit for discussions. This work was supported by a Rosalinde and Arthur Gilbert Foundation/American Federation for Aging Research research grant (I.S.), the Legacy Heritage Biomedical Program of the Israel Science Foundation (I.S.), the Israel Ministry of Health (I.S.), the National Institute of Psychobiology in Israel founded by the Charles E. Smith family (I.S.), and the Center for Nanoscience and Nanotechnology of Tel Aviv University (I.D.).

AUTHOR CONTRIBUTIONS

E.A., I.D., H.F., E.R. and I.S. designed, performed and analyzed experiments. H.F. wrote the program for image processing. G.D.C. provided the *App*$^{-/-}$ mice colony. I.S. designed and supervised the project. I.S., E.A. and I.D. wrote the manuscript.

Published online at http://www.nature.com/natureneuroscience/.
Reprints and permissions information is available online at http://www.nature.com/reprintsandpermissions/.

1. Haass, C. *et al.* Amyloid β-peptide is produced by cultured cells during normal metabolism. *Nature* **359**, 322–325 (1992).
2. Seubert, P. *et al.* Isolation and quantification of soluble Alzheimer's β-peptide from biological fluids. *Nature* **359**, 325–327 (1992).
3. Shoji, M. *et al.* Production of the Alzheimer amyloid β protein by normal proteolytic processing. *Science* **258**, 126–129 (1992).
4. De Strooper, B. & Annaert, W. Proteolytic processing and cell biological functions of the amyloid precursor protein. *J. Cell Sci.* **113**, 1857–1870 (2000).
5. Haass, C. Take five–BACE and the gamma-secretase quartet conduct Alzheimer's amyloid β-peptide generation. *EMBO J.* **23**, 483–488 (2004).
6. Kamenetz, F. *et al.* APP processing and synaptic function. *Neuron* **37**, 925–937 (2003).
7. Cirrito, J.R. *et al.* Synaptic activity regulates interstitial fluid amyloid-β levels in vivo. *Neuron* **48**, 913–922 (2005).
8. Cirrito, J.R. *et al.* Endocytosis is required for synaptic activity-dependent release of amyloid-β in vivo. *Neuron* **58**, 42–51 (2008).
9. Iwata, N., Higuchi, M. & Saido, T.C. Metabolism of amyloid-β peptide and Alzheimer's disease. *Pharmacol. Ther.* **108**, 129–148 (2005).
10. Selkoe, D.J. Clearing the brain's amyloid cobwebs. *Neuron* **32**, 177–180 (2001).
11. Iwata, N. *et al.* Presynaptic localization of neprilysin contributes to efficient clearance of amyloid-β peptide in mouse brain. *J. Neurosci.* **24**, 991–998 (2004).
12. Devault, A. *et al.* Amino acid sequence of rabbit kidney neutral endopeptidase 24.11 (enkephalinase) deduced from a complementary DNA. *EMBO J.* **6**, 1317–1322 (1987).
13. Terry, R.D. *et al.* Physical basis of cognitive alterations in Alzheimer's disease: synapse loss is the major correlate of cognitive impairment. *Ann. Neurol.* **30**, 572–580 (1991).
14. DeKosky, S.T. & Scheff, S.W. Synapse loss in frontal cortex biopsies in Alzheimer's disease: correlation with cognitive severity. *Ann. Neurol.* **27**, 457–464 (1990).
15. Hsieh, H. *et al.* AMPAR removal underlies Aβ-induced synaptic depression and dendritic spine loss. *Neuron* **52**, 831–843 (2006).
16. Jacobsen, J.S. *et al.* Early-onset behavioral and synaptic deficits in a mouse model of Alzheimer's disease. *Proc. Natl. Acad. Sci. USA* **103**, 5161–5166 (2006).
17. Shankar, G.M. *et al.* Natural oligomers of the Alzheimer amyloid-β protein induce reversible synapse loss by modulating an NMDA-type glutamate receptor-dependent signaling pathway. *J. Neurosci.* **27**, 2866–2875 (2007).
18. Shankar, G.M. *et al.* Amyloid-β protein dimers isolated directly from Alzheimer's brains impair synaptic plasticity and memory. *Nat. Med.* **14**, 837–842 (2008).

© 2009 Nature America, Inc. All rights reserved.
npg

19. Lesné, S. *et al.* A specific amyloid-β protein assembly in the brain impairs memory. *Nature* **440**, 352–357 (2006).
20. Hartley, D.M. *et al.* Protofibrillar intermediates of amyloid β-protein induce acute electrophysiological changes and progressive neurotoxicity in cortical neurons. *J. Neurosci.* **19**, 8876–8884 (1999).
21. Ye, C., Walsh, D.M., Selkoe, D.J. & Hartley, D.M. Amyloid β-protein induced electrophysiological changes are dependent on aggregation state: *N*-methyl-d-aspartate (NMDA) versus non-NMDA receptor/channel activation. *Neurosci. Lett.* **366**, 320–325 (2004).
22. Nimmrich, V. *et al.* Amyloid {β} oligomers (A{β}1–42 globulomer) suppress spontaneous synaptic activity by inhibition of P/Q-type calcium currents. *J. Neurosci.* **28**, 788–797 (2008).
23. Iwata, N. *et al.* Identification of the major Aβ1–42-degrading catabolic pathway in brain parenchyma: suppression leads to biochemical and pathological deposition. *Nat. Med.* **6**, 143–150 (2000).
24. Iwata, N. *et al.* Metabolic regulation of brain Aβ by neprilysin. *Science* **292**, 1550–1552 (2001).
25. Shirotani, K. *et al.* Neprilysin degrades both amyloid β peptides 1–40 and 1–42 most rapidly and efficiently among thiorphan- and phosphoramidon-sensitive endopeptidases. *J. Biol. Chem.* **276**, 21895–21901 (2001).
26. Ryan, T.A. *et al.* The kinetics of synaptic vesicle recycling measured at single presynaptic boutons. *Neuron* **11**, 713–724 (1993).
27. Murthy, V.N., Sejnowski, T.J. & Stevens, C.F. Heterogeneous release properties of visualized individual hippocampal synapses. *Neuron* **18**, 599–612 (1997).
28. Slutsky, I., Sadeghpour, S., Li, B. & Liu, G. Enhancement of synaptic plasticity through chronically reduced Ca2+ flux during uncorrelated activity. *Neuron* **44**, 835–849 (2004).
29. Zakharenko, S.S., Zablow, L. & Siegelbaum, S.A. Visualization of changes in presynaptic function during long-term synaptic plasticity. *Nat. Neurosci.* **4**, 711–717 (2001).
30. Zheng, H. *et al.* β-Amyloid precursor protein-deficient mice show reactive gliosis and decreased locomotor activity. *Cell* **81**, 525–531 (1995).
31. Debanne, D., Guerineau, N.C., Gahwiler, B.H. & Thompson, S.M. Paired-pulse facilitation and depression at unitary synapses in rat hippocampus: quantal fluctuation affects subsequent release. *J. Physiol. (Lond.)* **491**, 163–176 (1996).
32. Dobrunz, L.E. & Stevens, C.F. Heterogeneity of release probability, facilitation, and depletion at central synapses. *Neuron* **18**, 995–1008 (1997).
33. Selkoe, D.J. Alzheimer's disease is a synaptic failure. *Science* **298**, 789–791 (2002).
34. Zucker, R.S. & Regehr, W.G. Short-term synaptic plasticity. *Annu. Rev. Physiol.* **64**, 355–405 (2002).
35. Abbott, L.F. & Regehr, W.G. Synaptic computation. *Nature* **431**, 796–803 (2004).
36. Lisman, J.E., Raghavachari, S. & Tsien, R.W. The sequence of events that underlie quantal transmission at central glutamatergic synapses. *Nat. Rev. Neurosci.* **8**, 597–609 (2007).
37. Lisman, J.E. Bursts as a unit of neural information: making unreliable synapses reliable. *Trends Neurosci.* **20**, 38–43 (1997).
38. Katz, B. & Miledi, R. The role of calcium in neuromuscular facilitation. *J. Physiol. (Lond.)* **195**, 481–492 (1968).
39. Lou, X., Scheuss, V. & Schneggenburger, R. Allosteric modulation of the presynaptic Ca2+ sensor for vesicle fusion. *Nature* **435**, 497–501 (2005).
40. Dawson, G.R. *et al.* Age-related cognitive deficits, impaired long-term potentiation and reduction in synaptic marker density in mice lacking the β-amyloid precursor protein. *Neuroscience* **90**, 1–13 (1999).
41. Seabrook, G.R. *et al.* Mechanisms contributing to the deficits in hippocampal synaptic plasticity in mice lacking amyloid precursor protein. *Neuropharmacology* **38**, 349–359 (1999).
42. Ohno, M. *et al.* BACE1 deficiency rescues memory deficits and cholinergic dysfunction in a mouse model of Alzheimer's disease. *Neuron* **41**, 27–33 (2004).
43. Saura, C.A. *et al.* Loss of presenilin function causes impairments of memory and synaptic plasticity followed by age-dependent neurodegeneration. *Neuron* **42**, 23–36 (2004).
44. Puzzo, D. *et al.* Picomolar amyloid-β positively modulates synaptic plasticity and memory in hippocampus. *J. Neurosci.* **28**, 14537–14545 (2008).
45. Palop, J.J. *et al.* Aberrant excitatory neuronal activity and compensatory remodeling of inhibitory hippocampal circuits in mouse models of Alzheimer's disease. *Neuron* **55**, 697–711 (2007).
46. Brody, D.L. *et al.* Amyloid-β dynamics correlate with neurological status in the injured human brain. *Science* **321**, 1221–1224 (2008).
47. Hsia, A.Y. *et al.* Plaque-independent disruption of neural circuits in Alzheimer's disease mouse models. *Proc. Natl. Acad. Sci. USA* **96**, 3228–3233 (1999).
48. Scheff, S.W., DeKosky, S.T. & Price, D.A. Quantitative assessment of cortical synaptic density in Alzheimer's disease. *Neurobiol. Aging* **11**, 29–37 (1990).
49. Buckner, R.L. *et al.* Molecular, structural, and functional characterization of Alzheimer's disease: evidence for a relationship between default activity, amyloid, and memory. *J. Neurosci.* **25**, 7709–7717 (2005).

© 2009 Nature America, Inc. All rights reserved.

ONLINE METHODS

Hippocampal cell culture. Primary cultures of CA3-CA1 hippocampal neurons were prepared from newborn Wistar rats, $App^{-/-}$ and $App^{+/+}$ mice on postnatal days 0–2, as described[28]. The generation of the $App^{-/-}$ mice has been described[30]. The experiments were performed in mature (15–28 days *in vitro* (DIV)), high-density (synaptic density > 1.5 synapses per μm^2 of dendritic surface area) cultures. The cultures were grown in a culture medium (Gibco, 51200-038) with modified $[Mg^{2+}]_o$ (1.2 mM instead of 0.8 mM)[28]. All animal experiments were approved by the Tel Aviv University Committee on Animal Care.

Estimation of synaptic vesicle release based on FM dye staining. Synaptic vesicle release at single synapses was determined by counting the number of presynaptic vesicles turned over by a fixed number of action potentials, using the activity-dependent FM dye as a marker[27,28]. Briefly, action potentials in neurons were initiated by field stimulation (30 action potentials at 0.2 Hz) during dye loading, and the terminals, after undergoing vesicle exocytosis coupled to endocytosis, were stained by FM1-43 (see details in **Supplementary Fig. 1**). 10 μM FM1-43 (or 15 μM FM4-64, **Fig. 2a–d**) was present 5 s before and 20 s after the electrical stimulation. During FM loading and unloading, the extracellular solution contained (in mM): NaCl, 145; KCl, 3; glucose, 15; HEPES, 10; $MgCl_2$, 1.2; $CaCl_2$, 1.2; pH adjusted to 7.4 with NaOH. Kynurenic acid (0.5 mM) was added to prevent recurrent activity through blockage of excitatory postsynaptic responses during loading and unloading. After dye loading, external dye was washed away in Ca^{2+}-free solution containing ADVASEP-7 (0.1 mM; Sigma). To confirm that the fluorescent spots corresponded to release sites, we evoked activity at 2–5 Hz for 4 min during the unloading step to obtain release of dye–filled vesicles. The total amount of releasable fluorescence at each bouton (ΔF) was calculated from the difference between fluorescence after loading and after unloading ($\Delta F = F_{loading} - F_{unloading}$). The release probability (Pr) of individual terminals was calculated as $Pr = \Delta F/(N_{AP} \times F_Q)$, where F_Q is the estimated releasable fluorescence of a single synaptic vesicle, and N_{AP} is the number of action potentials applied during loading (see **Supplementary Fig. 3**). Under these conditions, application of 30 action potentials would make it possible to detect functional terminals with $Pr > 0.04$. The density of active terminals (D; **Figs. 1–7**) was calculated as N/A, where N is the number of FM$^+$ terminals per FM image, and A is the imaged area (except chronic thiorphan incubation, **Supplementary Fig. 10**, where A was dendrite area). The total presynaptic strength has been calculated as $S = \Delta F \times D$.

To determine the total presynaptic strength during burst patterns (S_{burst}), 30 action potentials were delivered in bursts consisting of 5 action potentials at regular frequency (10–100 Hz, at inter-burst intervals of 0.2–5 s) or in 'natural' burst patterns derived from extracellular recordings in the CA1 region of the hippocampus of running rats (provided by A. Lee and M. Wilson, unpublished data). To determine the sign and magnitude of short-term plasticity, we calculated S_{burst}/S_{single} over the same image area, whereas S_{single} was measured for the loading of 30 action potentials at 0.2 Hz.

Functional imaging and analysis. Images were obtained with an Olympus (FV300) confocal laser inverted microscope. The 488-nm line of an argon laser was used for excitation, and the emitted light was filtered using a 510-nm long-pass filter and detected by a photomultiplier. A 60 × 1.2 NA water-immersion objective was used for imaging. The confocal aperture was partially open and image resolution was 57–92 nm per pixel. The gain of the photomultiplier was adjusted to maximize the signal-to-noise ratio without causing saturation by the strongest signals. The image after FM dye unloading was subtracted from the initial image; thus, only those terminals containing activity-dependent releasable FM dye (~90% of total staining) were analyzed. FM$^+$ puncta were selected for further analysis by means of custom scripts written in ImagePro Plus (Media Cybernetics) and MATLAB (Mathworks) programs based on the following criteria: the fluorescence intensity (ΔF) was 2 s.d. above the mean background and the area of puncta was 0.1–2 μm^2. The FM$^+$ puncta were detected by applying a binary mask that was created from the ΔF image using adaptive thresholding. To analyze total presynaptic strength over synaptic population ($S = \Delta F \times D$), we created an individual binary mask for each image. To perform single synapse analysis comparing two images before and after treatment, we created a binary mask using the ΔF image that has the most synapses and applied it to both images. Centers of mass of detected FM$^+$ puncta were compared between two ΔF images to ensure analysis of the same synapses.

Transfections. Transient (18–24 h) cDNA transfections of APP_{695}^{YFP} (ref. 50) fusion protein were performed using Lipofectamine-2000 reagents in 11–13 DIV cultures.

Whole-cell recordings in hippocampal culture. Experiments were performed at room temperature in a recording chamber on the stage of a Zeiss Axiovert S100 microscope. Extracellular Tyrode solution contained (in mM): NaCl, 145; KCl, 3; glucose, 15; HEPES, 10; $MgCl_2$, 1.2; $CaCl_2$, 1.2; pH adjusted to 7.4 with NaOH. For measurement of mEPSCs (**Fig. 3**) and I/F curve (**Fig. 5f**), whole-cell patches with low-access resistance (<10 MΩ) were performed by membrane rupture. Whole-cell patches were recorded using the following intracellular solution (in mM): KGluconate, 120; KCl, 3; HEPES, 10; NaCl, 8; $CaCl_2$, 0.5; EGTA, 5; Mg^{2+}-ATP, 2; and GTP, 0.3; pH adjusted to 7.25 with KOH. Serial resistance was not compensated. For mEPSC recordings, tetrodotoxin (TTX; 1 μM, Alamon Labs), amino-phosphonopentanoate (AP-5; 50 μM, Sigma) and gabazine (30 μM, Tocris) were added to the Tyrode solution. Frequency versus current intensity curves were plotted by measuring the average rate of action potentials in current clamp during 100-ms long depolarizing steps of increasing intensity in the presence of synaptic blockers (50 μM AP-5, 20 μM DNQX and 30 μM gabazine).

For the experiments shown in **Figure 4f–h** and **5a**,**c**, we obtained perforated patch-clamp recordings. Perforated patch pipettes (2–3 MΩ resistance) were front-filled with a solution containing (in mM): KGluconate, 130; KCl, 4; HEPES, 10; NaCl, 8, EGTA, 0.4; pH adjusted to 7.2 with KOH and then back-filled with the same solution containing 150–200 ng ml^{-1} amphotericin B (Sigma). Dual perforated whole-cell data were recorded from two interconnected cultured hippocampal pyramidal neurons (**Fig. 4f**). 0.1 μM CNQX, blocking $EPSC_{AMPA}$ by 10%, was added to reduce spontaneous network activity in dual-patch recordings. This low concentration did not affect short-term plasticity measurements. The presynaptic cell was held in current-clamp mode, and a 10 ms current pulse (80–120 pA) induced action potential firing. The postsynaptic cells were held in voltage-clamp mode at −70 mV. Only neurons with monosynaptic connections were used. The access resistances of both pre- and post-synaptic neurons were monitored online and were typically 7–20 MΩ. Recordings with access resistances that exceeded 20 MΩ or that varied substantially were excluded from analysis.

To measure the excitation/inhibition (E/I) balance (**Fig. 5c**), sEPSCs and sIPSCs were isolated in the same cell based on reversal potentials of $GABA_A$ R-mediated and AMPAR-mediated currents, respectively. For these experiments, perforated patch pipettes were front-filled with a solution containing (in mM): CsOH, 127; D-gluconic acid, 127; CsCl, 4; HEPES, 10; NaCl, 8; EGTA, 0.4; pH adjusted to 7.25 with CsOH and then back–filled with the same solution containing 150–220 ng ml^{-1} amphotericin B. Given the intracellular and extracellular solutions used in the present study, the reversal potential for E (V_E) was close to +4 mV and V_I was close to −70 mV. Membrane holding potentials were corrected following data acquisition for the experimentally determined liquid junction potential (13 ± 2 mV). Signals were recorded using a MultiClamp 700A amplifier, digitized by DigiData1440A (Molecular Devices) at 10 kHz, and filtered at 2 kHz. Electrophysiological data were analyzed using MiniAnalysis (Synaptosoft) for miniature and spontaneous currents or potentials, and in pClamp10 (Molecular Devices) for EPSCs evoked presynaptically.

Electrophysiology of hippocampal slices. Coronal hippocampal slices (400 μm) were prepared from 1- to 2-month-old Wistar rats in a cold (4 °C) storage buffer containing (in mM): sucrose, 206; KCl, 2; MgSO4, 2; NaH2PO4, 1.25; NaHCO3, 26; CaCl2, 1; MgCl2, 1; glucose, 10. The slicing procedure was preformed using a Leica VT1200 vibratome. Slices were transferred to a submerged recovery chamber at room temperature containing oxygenated (95% O_2 and 5% CO_2) artificial cerebrospinal fluid (ACSF) for 1 h before recording. The ACSF contained, in mM: NaCl, 125; KCl, 2.5; $CaCl_2$, 1.2; $MgCl_2$, 1.2; $NaHCO_3$, 25; NaH_2PO_4, 1.25; glucose, 25. Experiments were performed at room temperature in a recording chamber on the stage of a Zeiss Axiovert S100 microscope. Extracellular fEPSPs were recorded with a glass pipette containing ACSF (1–2 MΩ) from the CA1 stratum radiatum, using a MultiClamp700A amplifier (Molecular Devices). Stimulation was evoked in the Schaffer collateral-commissural pathway and delivered through a glass suction electrode (10–20 μm tip) filled with ACSF. fEPSPs were induced by repetitive stimulations at 0.033 Hz or by bursts (each burst contains 5 action potentials, inter-spike interval 10 ms, inter-burst interval 30 s). The relationship between input (peak amplitude of the fiber volley, 0.033 Hz) and output (fEPSP amplitude

© 2009 Nature America, Inc. All rights reserved.

and slope) was calculated to estimate basal synaptic transmission. fEPSPs were analyzed by pClamp10 software (Molecular Devices).

ELISA of Aβ. Concentrations of rat $A\beta_{40}$ and $A\beta_{42}$ in fresh extracellular medium were determined by sandwich ELISA using highly sensitive commercial kits (Wako) according to the manufacturer's instructions. BNT77 was used as a capture antibody, BA27 as antibody for $A\beta_{40}$, and BC05 for $A\beta_{42}$. Only fresh samples were used. In each experiment, media from four coverslips were mixed and analyzed.

Chemical reagents. FM1-43 and Advasep-7 were purchased from Biotium, thiorphan and AP-5 from Sigma, 4G8 from Signet, AF1126 from R & D Systems, BACE1 inhibitor IV and L-685,458 from Calbiochem, $A\beta_{1\text{-}40}$ and $A\beta_{1\text{-}42}$ from Bachem, TTX from Alamon Labs, and gabazine and CNQX from Tocris. Thiorphan solution was stored at 1 mM in ACSF solution containing 1 mM ascorbic acid to prevent thiorphan oxidation[23]. Equal amounts of ascorbic acid were added to control samples before thiorphan was applied.

Statistical analysis. Error bars shown in the figures represent s.e.m. (s.e.m.). Student's paired *t*-tests were used in all the experiments where the effect of thiorphan (or other compounds) was tested in the same cell/synapse ($^{*}P < 0.05$; $^{**}P < 0.01$; $^{***}P < 0.001$). Unpaired *t*-tests were used to compare different populations of synapses. A one-way ANOWA Kruskal-Wallis non-parametric test was used to compare several populations of synapses. The nonparametric Spearman test was used for correlation analysis. For comparison of mEPSC amplitude or frequency under different conditions, 200 mEPSCs were randomly selected for each cell and pooled for each condition. A Kolmogorov-Smirnov (K-S) test was used to compute differences in mEPSC amplitude and frequency across the pooled datasets.

50. Kaether, C., Skehel, P. & Dotti, C.G. Axonal membrane proteins are transported in distinct carriers: a two-color video microscopy study in cultured hippocampal neurons. *Mol. Biol. Cell* **11**, 1213–1224 (2000).

© 2009 Nature America, Inc. All rights reserved.

doi:10.1038/nn.2433